Electronic structure of optimally doped pnictide $Ba_{0.6}K_{0.4}Fe_2As_2$: a comprehensive angle-resolved photoemission spectroscopy investigation

2011 J. Phys.: Condens. Matter 23 135701

(http://iopscience.iop.org/0953-8984/23/13/135701)

J. Phys.: Condens. Matter **23** (2011) 135701 (6pp) doi:10.1088/0953-8984/23/13/135701

Electronic structure of optimally doped pnictide $Ba_{0.6}K_{0.4}Fe_2As_2$: a comprehensive angle-resolved photoemission spectroscopy investigation

H Ding[1], K Nakayama[2], P Richard[1,3], S Souma[3], T Sato[2,4], T Takahashi[2,3], M Neupane[5], Y-M Xu[5,6], Z-H Pan[7], A V Fedorov[8], Z Wang[5], X Dai[1], Z Fang[1], G F Chen[9], J L Luo[1] and N L Wang[1]

[1] Beijing National Laboratory for Condensed Matter Physics, and Institute of Physics, Chinese Academy of Sciences, Beijing 100190, People's Republic of China
[2] Department of Physics, Tohoku University, Sendai 980-8578, Japan
[3] WPI Research Center, Advanced Institute for Materials Research, Tohoku University, Sendai 980-8577, Japan
[4] TRIP, Japan Science and Technology Agency (JST), Kawaguchi 332-0012, Japan
[5] Department of Physics, Boston College, Chestnut Hill, MA 02467, USA
[6] Materials Sciences Division, Lawrence Berkeley National Laboratory, Berkeley, CA 94720, USA
[7] Condensed Matter Physics and Materials Science Department, Brookhaven National Laboratory, Upton, NY 11973-5000, USA
[8] Advanced Light Source, Lawrence Berkeley National Laboratory, Berkeley, CA 94720, USA
[9] Department of Physics, Renmin University, Beijing 100872, People's Republic of China

E-mail: dingh@iphy.ac.cn and p.richard@iphy.ac.cn

Received 22 December 2010
Published 17 March 2011
Online at stacks.iop.org/JPhysCM/23/135701

Abstract
The electronic structure of the Fe-based superconductor $Ba_{0.6}K_{0.4}Fe_2As_2$ is studied by means of angle-resolved photoemission. We identify dispersive bands crossing the Fermi level forming hole-like (electron-like) Fermi surfaces (FSs) around Γ (M) with nearly nested FS pockets connected by the antiferromagnetic wavevector. Compared to band structure calculation findings, the overall bandwidth is reduced by a factor of 2 and the low energy dispersions display even stronger mass renormalization. Using an effective tight banding model, we fitted the band structure and the FSs to obtain band parameters reliable for theoretical modeling and calculation of physical quantities.

(Some figures in this article are in colour only in the electronic version)

1. Introduction

The recent discovery of superconductivity [1] in iron pnictides has opened a new route to high temperature superconductivity beyond the cuprates. It is now widely believed that the multiband nature of this material is important, pertaining to the superconducting instability in the doped compound and the antiferromagnetic (AF) spin density wave (SDW) instability [2] leading to Dirac cone dispersion in the parent compound [3–5]. The knowledge of the electronic band structure and the Fermi surface (FS) topology is critical to understand the underlying physics. Most first principle band theory calculations, such as local density approximation (LDA) [6–8], have predicted that five bands of the Fe 3d t_{2g} complex cross the Fermi level (E_F) and form three hole-like FSs centered at the zone center (Γ) and two electron-like FS centered at the zone corner (M). However, inconsistencies in the predicted band structure remain [9]. More seriously,

the optimal As position calculated in LDA is quite different (more than 10%) from the experimental values [9]. On the experimental side, angle-resolved photoemission spectroscopy (ARPES) studies [10–17, 19] have observed several dispersive bands and FSs, showing some consistencies with LDA calculations. However, some major discrepancies exist and a quantitative comparison is lacking. In particular, there is no consensus regarding the band structure and FS near the M point ((π, π) in the 1 Fe unit cell representation). In order to resolve these controversies and obtain comprehensive knowledge of the electronic structure of the iron pnictides, we have carried out a systemic ARPES study on an optimally hole-doped superconductor $Ba_{0.6}K_{0.4}Fe_2As_2$.

2. Experiment

The high-quality single crystals of $Ba_{0.6}K_{0.4}Fe_2As_2$ used in this study were grown by the flux method [20, 21]. These are the same samples used to determine the FS dependent nodeless superconducting gaps that close at the bulk $T_c = 37$ K [10]. Low energy electron diffraction (LEED) on a mirror-like cleaved surface shows a sharp 1×1 pattern without reconstruction down to 20 K. A previous STM and LEED study [22] on the parent compound $BaFe_2As_2$ has demonstrated that the terminating layer of cleaved crystals is the Ba layer, with half of the Ba atoms remaining on one side of the sample macroscopically, as required for electrostatic stability since the Ba layer is shared between two equivalent FeAs layers. Their quantitative analysis indicates that the surface structure of this material represents the low temperature orthorhombic phase in bulk, without surface reconstruction. The bulk representativity of the electronic structure of $Ba_{0.6}K_{0.4}Fe_2As_2$ seen by ARPES is further supported by: (i) a surface doping consistent with the bulk [10, 18]; (ii) a k_z-dependence of the electronic structure [19], in sharp contrast to a surface state; (iii) a doping evolution of the Fermi surface consistent with Luttinger's theorem [23]; (iv) a band structure similar to LDA predictions, as will be shown below; and (v) a gap closing at the bulk T_c [10, 18]. High-resolution (4–20 meV) ARPES measurements were performed in the photoemission laboratory of Tohoku University using a microwave-driven helium source ($h\nu = 21.218$ eV), and several synchrotron beamlines in the Synchrotron Radiation Center and the Advanced Light Source in the US, and the Photon Factory in Japan with photon energies ranging from 20 to 100 eV to selectively enhance different band features of this multiband system. Samples were cleaved *in situ* at 10–40 K and measured at 7–150 K in a working vacuum better than 1×10^{-10} Torr.

3. Results and discussion

We start with a wide energy spectrum (figure 1(a)) that includes shallow core levels and the valence band, which can yield valuable information on the valence and chemical environment of the constituent elements. The strong double peaks at the binding energies of 40.4 and 41.1 eV are from As $3d_{5/2}$ and $3d_{3/2}$, the same as the 3d core levels of As in bulk GaAs (40.4 and 41.4 eV) [24]. However, unlike GaAs (110) that has a surface component in As 3d core levels, $Ba_{0.6}K_{0.4}Fe_2As_2$ shows no clear evidence for a second component of As 3d, suggesting no major surface modification involving the As atoms. We have also identified several other core levels, such as Fe 3p (52.4, 53.0 eV), K 3s (33.0 eV) and 3p (17.8 eV), Ba 5s (29.7 eV) and 5p (14.2, 16.2 eV). In addition, there is a weak but well-defined peak at 12 eV, as shown in the inset of figure 1(a). which has also been observed in our measurements of the parent compounds $BaFe_2As_2$ and $SrFe_2As_2$. While it may be due to the As 4s shallow core level, we note that a peak at a similar binding energy was observed in divalent iron compounds, such as FeO [25], and attributed to a satellite state of the Fe $3d^5$ configuration involving different final states in the photoemission process itself.

The valence band shows a strong photon energy dependence. Comparing energy distribution curves (EDCs) measured at 100 eV (enhancing the intensity of Fe 3d) and the ones measured at 21.2 eV (enhancing the intensity of As 4p), one can conclude that the strong peak within 1 eV from E_F is mostly from Fe 3d orbitals, and the states below it are mostly from As 4p, in agreement with LDA calculations [26]. The variation of the valence band intensity when the photon energy is scanned through the Fe 3p absorption edge (~56 eV) can be seen in figure 1(b). Following a common practice in photoemission [25], we also plot in figure 1(b) the difference between EDCs measured at 56 eV (at resonance) and 52 eV (below resonance), which corresponds mostly to Fe 3d states since the intensity of other orbitals is not expected to change drastically over this narrow photon energy window[10]. The difference curve shows a sharp peak at E_F corresponding to the coherent Fe 3d orbitals, and a broad peak centered at ~7 eV which can be regarded as the incoherent part of the Fe 3d states. The assignment of coherent and incoherent components is also supported by the observation in figure 1(d) of the 'anti-resonance' profile of the coherent part and the Fano-like resonance profile for the incoherent part at 7 eV due to the super Coster–Kronig Fe 3p–3d Auger transition, which is similar to what has been observed in FeO [25]. The large incoherent component of Fe 3d at high binding energy is an indication of relatively strong correlation effects in this material. The correlation effects are also reflected from the observation that the coherent part of Fe 3d is narrowed to 1 eV below E_F (see figure 1(c)) from the 2 eV range predicted by LDA, which is inline with dynamic mean field theory (DMFT) calculations that assume strong correlations [27, 28].

Within the coherent Fe 3d region, we observe several dispersive bands as shown in figure 2, which displays band dispersions along several high symmetry directions (Γ–M, Γ–X and M–X) determined using the EDCs (figures 2(a) and (b)), E versus k intensity plots (figures 2(c) and (d)), second derivative plots (figure 2(e)), and the extracted EDC peak position (figure 2(f)). We also plot the band dispersion from our LDA calculations [8] at this doping level. The LDA bands, when normalized (divided) by a factor of 2, show overall agreement with the observed bands, especially

[10] We caution that some ordinate Auger intensity will be also included in the difference curve.

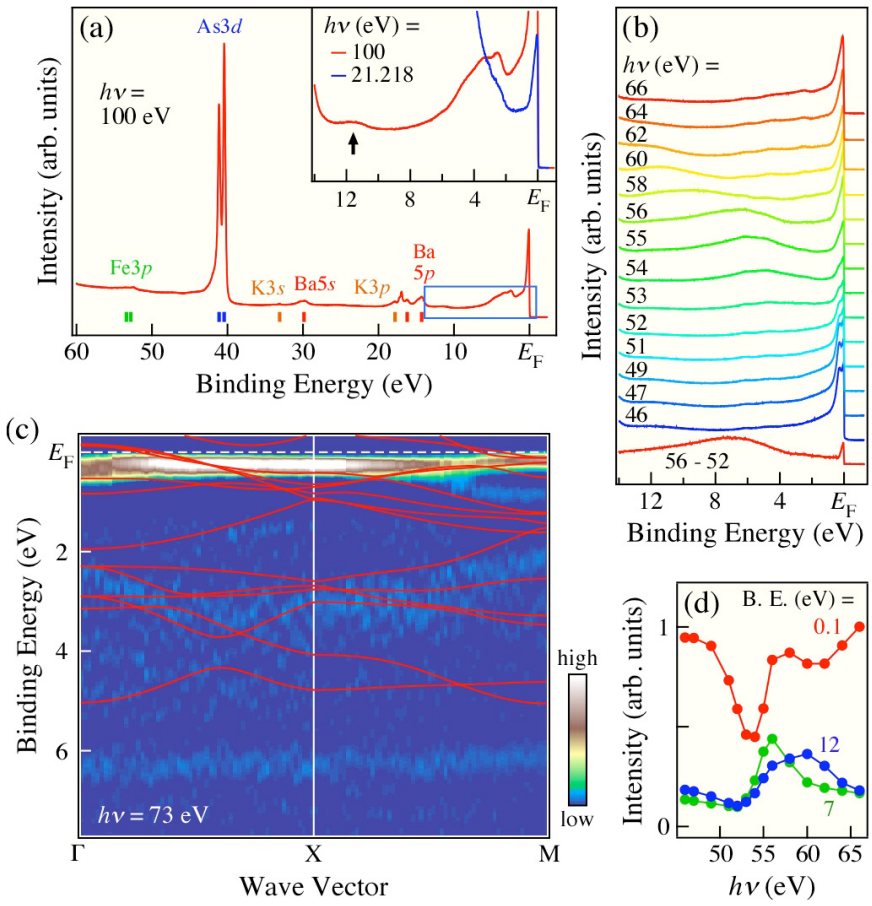

Figure 1. (a) Wide range EDC near Γ showing shallow core levels marked by vertical bars above the x-axis. The inset magnifies the valence band and a possible satellite peak at ∼12 eV, and highlights the difference between spectra taken at 100 and 21.2 eV. (b) Valence band near Γ measured at different photon energies (46–66 eV). All EDCs are normalized by the photon flux. (c) Intensity plot of second derivatives of spectra along Γ–X and X–M. LDA bands (red lines) are plotted for comparison. (d) Photon energy dependence of the EDC intensity shown in figure 1(b) obtained at binding energies 0.1, 7, and 12 eV.

for the high energy (0.2–0.6 eV) branches, as indicated in figure 2(f). This band narrowing factor of 2, similar to an earlier ARPES observation in a related pnictide (LaFeOP) [15], indicates the importance of correlation effects as seen in the multiorbital cobaltates [29]. However, we observe additional mass renormalization for the lower energy branches (below 0.2 eV), as shown in figure 2(f), which will be discussed in more details below, suggesting stronger and possibly band or energy dependent correlation effects.

In order to accurately determine the low energy band structure and the FS, we have performed high-resolution ARPES measurements in the vicinity of E_F, as shown in figure 3. Figure 3(a) an E versus k intensity plot near the Γ point, which clearly shows two dispersing bands (α and β) forming two hole-like FS pockets around Γ. This spectrum is measured in the superconducting state where the quasiparticle (QP) peak width is narrower and the separation of the α and β bands more visible. Recent studies of the k_z-dependence of the band structure near the Γ point showed evidence for a third hole band almost degenerate with the α band [19, 30]. We have observed the top of the α band at the Γ point by dividing out the Fermi function from the high temperature ($T = 150$ K) data. As shown in figure 3(b), this procedure unmasks the spectrum within a few k_BT above E_F, showing a clear parabola with a band top situated at ∼20 meV above E_F. This band top is much lower than the value of ∼120 meV predicted by LDA calculations.

The band structure near M has been controversial. While LDA predicts two electron-like FSs around M, earlier ARPES reports claimed to have observed a hole-like dispersion [14, 16]. Using high-resolution ARPES, we identify in figures 3(c) and (d) two electron-like bands (labeled as γ and δ bands) with band bottoms at ∼15 and 60 meV, respectively. The energy difference from the top of the α band to the bottom of the γ band is about 35 meV, much smaller than the ∼200 meV predicted by LDA [26]. In addition, we observe in figure 3(c) a third band dispersing toward E_F when moving from Γ to M, intersecting with the δ band in the vicinity of E_F. As can be seen in figure 4(e), LDA predicts the anti-crossing (or a Dirac point) of the two bands near M. However, it occurs at a much higher binding energy (∼120 meV). This uplift of the Dirac point also creates a 'bright' spot with high intensity at E_F observed in previous ARPES measurements [10, 14, 16].

The measured FSs and band structure are summarized in figure 4. By measuring many cuts in the Brillouin zone (BZ), we have obtained the FSs of $Ba_{0.6}K_{0.4}Fe_2As_2$. Figure 4(a)

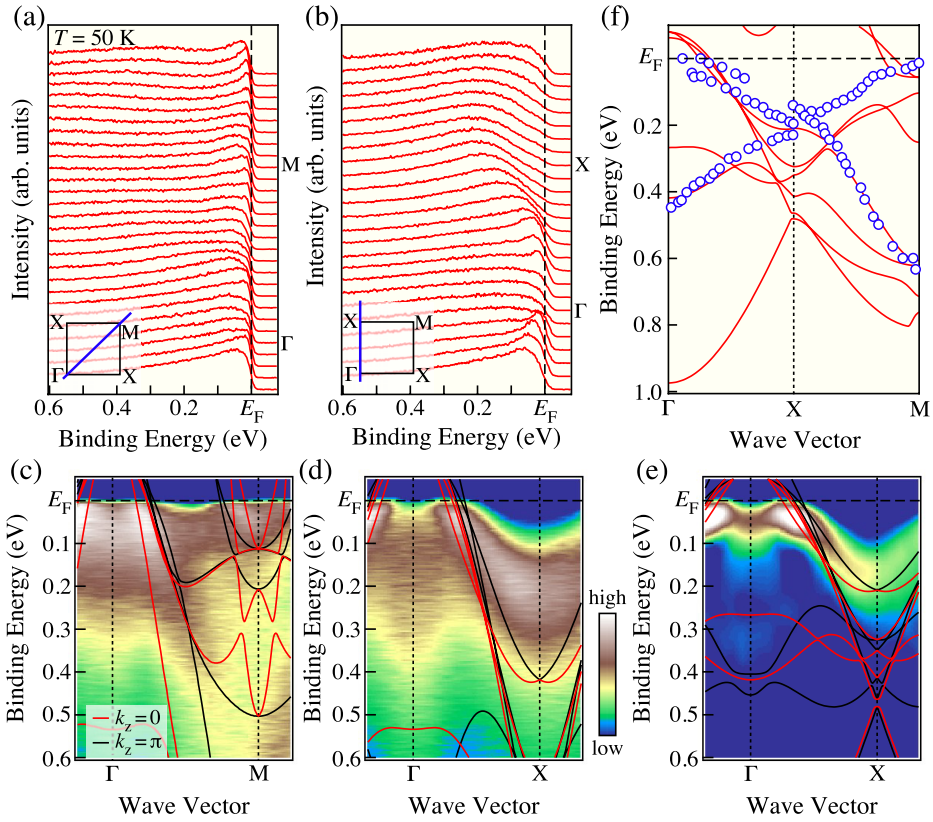

Figure 2. EDCs measured at 50 K along (a) Γ–M and (b) Γ–X ($h\nu = 21.2$ eV). Intensity plots of the same spectra along (c) Γ–M and (d) Γ–X. LDA calculated bands at $k_z = 0$ (red) and $k_z = \pi$ (black) are plotted for comparison. (e) Intensity plot of second derivatives of the spectra along Γ–X in comparison with normalized LDA bands (divided by 2). (f) Extracted band positions (blue circles) measured at 45 eV along Γ–X–M with comparisons to the same normalized LDA bands.

displays the ARPES intensity integrated within $E_F \pm 10$ meV, where the high intensity contours map out the FSs. The dots mark the k_F points of the dispersive bands obtained from both momentum distribution curves (MDCs) and EDCs. These k_F points, coinciding with the high intensity contours, clearly show four FS sheets. The hole-like α and β FSs centered at Γ enclose areas of 4% and 18% of the Brillouin zone (BZ), while the electron-like γ and δ FSs centered at M have areas of 2% and 4%, respectively. According to Luttinger's theorem on two-dimensional (2D) FS sheets and taking into account the existence of a third hole-like FS almost degenerate with the α FS [19, 30], the observed FS sheets correspond to 20% hole/Fe. This value is consistent with the nominal K concentration of 40% per (Ba, K)Fe_2As_2 formula unit, which is equivalent to 20% hole/Fe.

Figure 4(b) shows a comparison of the measured dispersion along Γ–M and Γ–X with the LDA bands normalized by a factor of 2. While there is a fairly good agreement on the Fermi crossing points (k_F), the Fermi velocity (v_F) is further renormalized. The values of v_F from ARPES and LDA are listed in figure 4(c). Most low energy bands have a mass renormalization greater than 4, significantly larger than the overall band narrowing. This additional renormalization of low energy excitations, which has also been observed in both cuprates [31] and cobaltates [29], points to an enhanced self-energy effect near E_F. Possible causes include band or energy dependent correlation effects, low energy modes or fluctuations, and band hybridization. Independent of its microscopic origin, the small Fermi velocity has an important consequence on the superconducting coherence length, which can be estimated from the BCS relation $\xi = \frac{\hbar v_F}{\pi \Delta}$. From the values of v_F and the measured superconducting gaps [10], we estimate that the coherence length is about 9–14 Å, which agrees well with the value (∼12 Å) obtained from the c-axis upper critical field [32]. It is remarkable that the superconducting coherence length in this pnictide is much smaller than conventional BCS superconductors and surprisingly close to that of the cuprate superconductors [33].

A set of basic band parameters of this material constitutes an important starting point for microscopic and phenomenological theories of its unusual superconductivity and other instabilities. After determining the band structure and the FSs, we can extract the dispersion parameters. Here we adapt a simple tight-binding-like band structure proposed previously [34]: $E^{\alpha,\beta}(k_x, k_y) = E_0^{\alpha,\beta} + t_1^{\alpha,\beta}(\cos k_x + \cos k_y) + t_2^{\alpha,\beta} \cos k_x \cos k_y$, and $E^{\gamma,\delta}(k_x, k_y) = E_0^{\gamma,\delta} + t_1^{\gamma,\delta}(\cos k_x + \cos k_y) + t_2^{\gamma,\delta} \cos(k_x/2) \cos(k_y/2)$. Under mild constraints for the unoccupied bands which are not accessible by ARPES, we obtain the band parameters for the four observed bands which are listed in the table in figure 4(b). As shown in figures 4(b) and (d), the FS contours and the band dispersions generated from these parameters match remarkably well with

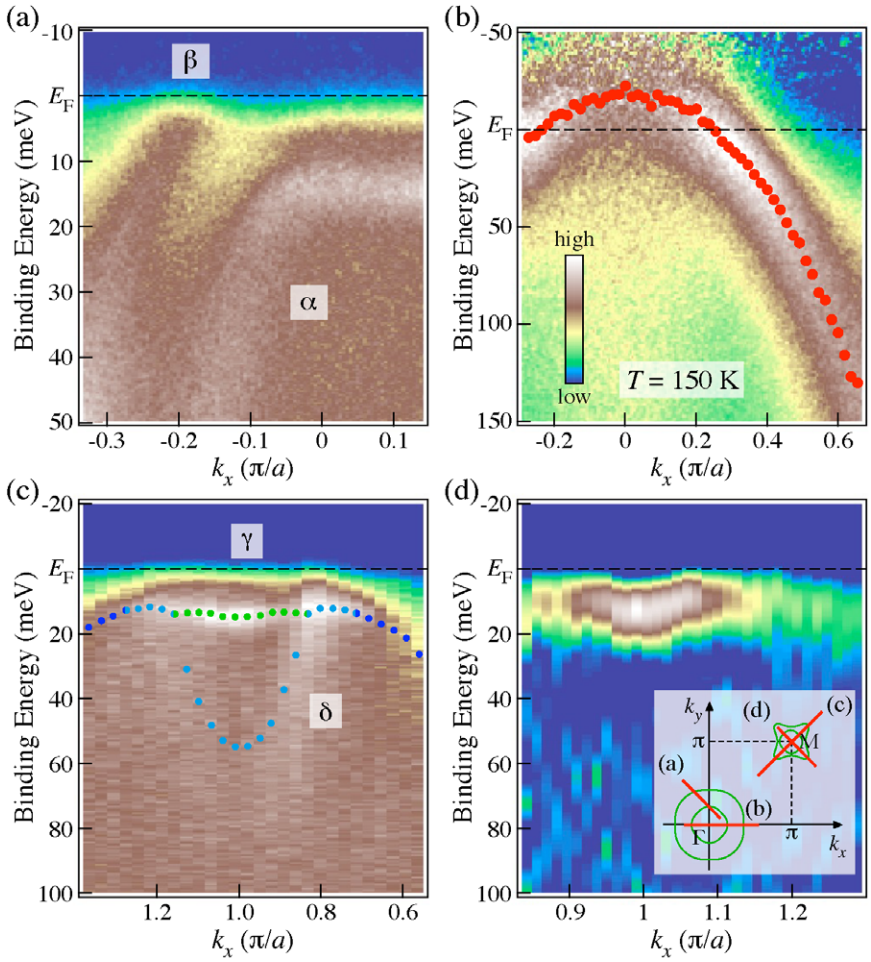

Figure 3. (a) Intensity plot near Γ measured at low temperature ($T = 15$ K). (b) Intensity plot near Γ measured at high temperature ($T = 150$ K) divided by the Fermi function. Red dots are band positions extracted from EDC peaks. (c) Intensity plot near M measured at 15 K. Dots are EDC peak positions. (d) Intensity plot of second derivatives of spectra near M. The inset indicates measurement locations in the Brillouin zone for panels (a)–(d).

the observed ones. Note that the fitted FSs for the (γ, δ) bands in the vicinity of M are two ellipses without hybridization. The latter splits the two bands and gives rise to the observed outer (δ) and inner (γ) FSs. As seen clearly in figure 4(d), the α FS, when shifted by the (π, π) wavevector defined in the reconstructed BZ, overlaps well with the δ and γ FSs, revealing good FS quasi-nesting by the AF wavevector observed in the parent compound [2]. Combined with the observation of nearly identical superconducting gaps on the α, δ, and γ FSs [10, 18] and of a band-selective electron-mode coupling [35] in the same material, this result reinforces the notion that interband scattering among the nested FSs plays a dominant role in the pairing interaction [36–41].

The effective band parameters enable an estimate of the effective masses of the low energy bands, whose average values along the FSs are: $m^*_\alpha = 4.8$, $m^*_\beta = 9.0$, $m^*_\gamma = 1.3$, $m^*_\delta = 1.3$, in units of the free electron mass. The Sommerfeld parameter for the electronic specific heat is given by $\gamma = \pi N_A k_B^2 a^2 m^*/3\hbar^2$, where $a = 3.92$ Å is the lattice parameter and N_A is Avogadro's constant. The parameters derived from our model lead to 7.2, 13.6, 2, and 2 mJ K^{-2} mol^{-1} for the α, β, γ, δ bands, respectively. Using these approximated values, the total value of the γ coefficient, assuming a doubly degenerate α band, is estimated to ∼32 mJ K^{-2} mol^{-1}. Both this approximation and the value of ∼63 mJ K^{-2} mol^{-1} [42] estimated by specific heat for the normal state γ coefficient in superconducting $Ba_{0.6}K_{0.4}Fe_2As_2$ are much larger than the value (∼9 mJ K^{-2} mol^{-1}) calculated using LDA [26], most likely due to the unusually strong mass renormalization. The measured γ coefficient in the parent compound $SrFe_2As_2$ is 6.5 mJ K^{-2} mol^{-1} [21]. The significant reduction is likely due to the gapping of large portions of FS sheets [3, 43, 44].

4. Conclusion

In conclusion, we have determined the band structure and the FS of the optimally doped Fe-based superconductor $Ba_{0.6}K_{0.4}Fe_2As_2$. Hole-like FSs around Γ and electron-like FSs around M are clearly observed. The two electron-like FSs around M are consistent with the unexpected hybridization of the two overlapping orthogonal elliptic FSs, which are nearly nested with the inner hole-like (α) FS via the (π, π) AF wavevector. The overall bandwidth is renormalized by a factor of 2, while the low energy dispersions acquire an even

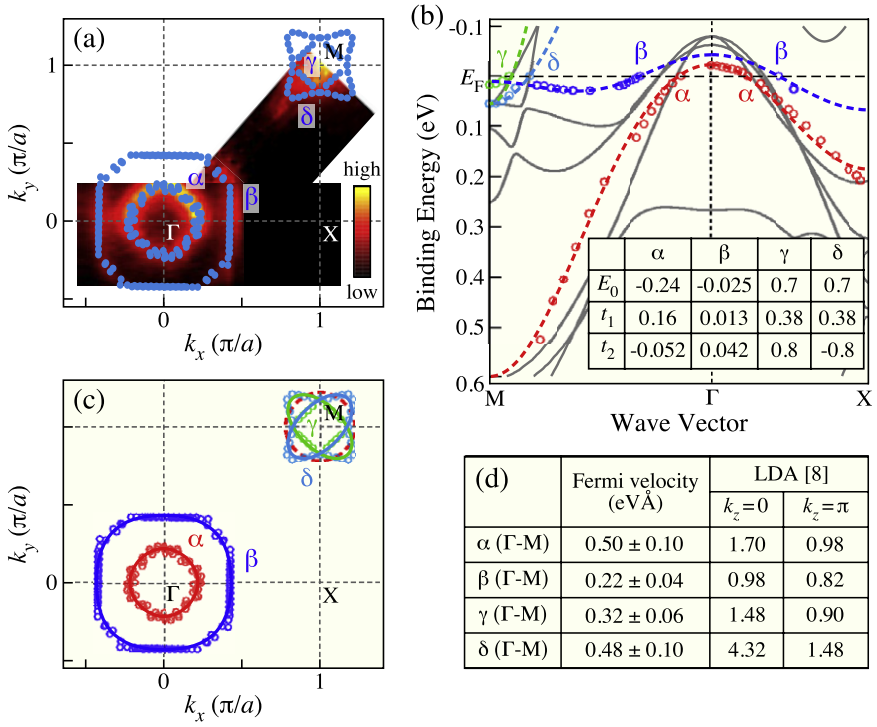

	α	β	γ	δ
E_0	-0.24	-0.025	0.7	0.7
t_1	0.16	0.013	0.38	0.38
t_2	-0.052	0.042	0.8	-0.8

(d)	Fermi velocity (eVÅ)	LDA [8]	
		$k_z=0$	$k_z=\pi$
α (Γ-M)	0.50 ± 0.10	1.70	0.98
β (Γ-M)	0.22 ± 0.04	0.98	0.82
γ (Γ-M)	0.32 ± 0.06	1.48	0.90
δ (Γ-M)	0.48 ± 0.10	4.32	1.48

Figure 4. (a) FSs in the 2D BZ obtained from integrated intensity within $E_F \pm 10$ meV (false color plot) and Fermi crossing points (blue dots) obtained from MDC and EDC dispersions. (b) Measured band dispersion (circles) along Γ–M and Γ–X, compared with the LDA bands normalized by a factor of 2 (solid lines), and tight-binding fits (dashed lines). The inset table lists parameters of tight-binding bands. (c) Measured FS (circles) and fitted tight-binding curves (solid lines). The dashed line is the fitted α FS shifted by (π, π). (d) Table of measured and calculated Fermi velocities along Γ–M.

stronger renormalization effect that implies a much enhanced specific heat coefficient $\gamma \sim 32$ mJ K^{-2} mol^{-1} calculated using the tight-binding band parameters obtained from fitting the observed electronic structure.

Acknowledgments

This work was supported by grants from the Chinese Academy of Sciences, NSF, Ministry of Science and Technology of China, JSPS, TRIP-JST, CREST-JST, MEXT of Japan, and NSF (DMR-0800641, DMR-0704545), DOE (DEFG02-99ER45747) of the US. This work is based upon research conducted at the Synchrotron Radiation Center supported by NSF DMR-0537588, and the Advanced Light Source supported by DOE No. DE-AC02-05CH11231.

References

[1] Kamihara Y *et al* 2008 *J. Am. Chem. Soc.* **130** 3296
[2] de la Cruz C *et al* 2008 *Nature* **453** 899
[3] Richard P *et al* 2010 *Phys. Rev. Lett.* **104** 137001
[4] Harrison N and Sebastian S E *et al* 2009 *Phys. Rev.* B **80** 224512
[5] Ran Y 2009 *Phys. Rev.* B **79** 014505
[6] Singh D J and Du M H 2008 *Phys. Rev. Lett.* **100** 237003
[7] Ma F and Lu Z-Y 2008 *Phys. Rev.* B **78** 033111
[8] Xu G *et al* 2008 *Europhys. Lett.* **84** 67015
[9] Mazin I I *et al* 2008 *Phys. Rev.* B **78** 085104
[10] Ding H *et al* 2008 *Europhys. Lett.* **83** 47001
[11] Kondo T *et al* 2008 *Phys. Rev. Lett.* **101** 147003
[12] Yang L X *et al* 2009 *Phys. Rev. Lett.* **102** 107002
[13] Liu C *et al* 2008 *Phys. Rev. Lett.* **101** 177005
[14] Zhao L *et al* 2008 *Chin. Phys. Lett.* **25** 4402
[15] Lu D H *et al* 2008 *Nature* **455** 81
[16] Zabolotnyy V B *et al* 2009 *Nature* **457** 569
[17] Wray L *et al* 2008 *Phys. Rev.* B **78** 184508
[18] Nakayama K *et al* 2009 *Europhys. Lett.* **85** 67002
[19] Xu Y-M *et al* 2011 *Nat. Phys.* **7** 198
[20] Rotter M *et al* 2008 *Phys. Rev. Lett.* **101** 107006
[21] Chen G F *et al* 2008 *Phys. Rev.* B **78** 224512
[22] Nascimento V B *et al* 2009 *Phys. Rev. Lett.* **103** 076104
[23] Nakayama K *et al* 2011 *Phys. Rev.* B **83** 020501
[24] Eastman D E *et al* 1980 *Phys. Rev. Lett.* **45** 656
[25] Lad R J and Henrich V E 1989 *Phys. Rev.* B **39** 13478
[26] Ma F *et al* 2010 *Front. Phys. China* **5** 150
[27] Haule K *et al* 2008 *Phys. Rev. Lett.* **100** 226402
[28] Craco L *et al* 2008 *Phys. Rev.* B **78** 134511
[29] Yang H-B *et al* 2005 *Phys. Rev. Lett.* **95** 146401
[30] Zhang Y *et al* 2010 *Phys. Rev. Lett.* **105** 117003
[31] Valla T *et al* 1999 *Science* **285** 2110
[32] Welp U *et al* 2009 *Phys. Rev.* B **79** 094505
[33] Pan S H *et al* 2001 *Nature* **413** 282
[34] Korshunov M M and Eremin I 2008 *Phys. Rev.* B **78** 140509(R)
[35] Richard P *et al* 2009 *Phys. Rev. Lett.* **102** 047003
[36] Mazin I I *et al* 2008 *Phys. Rev. Lett.* **101** 057003
[37] Kuroki K *et al* 2008 *Phys. Rev. Lett.* **101** 087004
[38] Wang F *et al* 2009 *Phys. Rev. Lett.* **102** 047005
[39] Seo K *et al* 2008 *Phys. Rev. Lett.* **101** 206404
[40] Yao Z J, Li J X and Wang Z D 2009 *New J. Phys.* **11** 025009
[41] Cvetkovic V and Tesanovic Z 2009 *Europhys. Lett.* **85** 37002
[42] Mu G *et al* 2009 *Phys. Rev.* B **79** 174501
[43] Dong J *et al* 2008 *Europhys. Lett.* **83** 27006
[44] Sebastian S E *et al* 2008 *J. Phys.: Condens. Matter* **20** 422203